Applied Surface Science 447 (2018) 471–478

Contents lists available at ScienceDirect

Applied Surface Science

journal homepage: www.elsevier.com/locate/apsusc

Full Length Article

Electrochromic behavior of WO_3 thin films prepared by GLAD

Jiali Yuan [a,b,c], Bin Wang [a,*], Hu Wang [a], Yingjie Chai [a], Yaxue Jin [a,b], Hongji Qi [a], Jianda Shao [a,*]

[a] Key Laboratory of Materials for High Power Laser, Shanghai Institute of Optics and Fine Mechanics, Chinese Academy of Sciences, Shanghai 201800, PR China
[b] University of Chinese Academy of Sciences, Beijing 100049, PR China
[c] ShanghaiTech University, Shanghai 201210, China

ARTICLE INFO

Article history:
Received 30 October 2017
Revised 26 March 2018
Accepted 31 March 2018
Available online 3 April 2018

Keywords:
GLAD
Annealing treatment
Electrochromic property
Tunable angular selectivity

ABSTRACT

WO_3 thin films fabricated by glancing angle deposition (GLAD) are proposed as excellent electrochromic coatings with favorable ion diffusion. A ~ 500-nm film prepared by GLAD had a relatively large transmittance modulation. The crystallization structure, surface morphology, chemical state, optical and electrochromic properties of WO_3 thin films were systematically characterized upon annealing treatment. Compared with annealed WO_3 porous nanostructured films, the amorphous as-deposited films exhibited a high coloration efficiency and stable reversibility. Furthermore, the GLAD WO_3 films exhibit the tunable angular selectivity under illumination with p-polarized light because of the birefringence, which could extend the application range of nanostructured films in the electrochromic field.

1. Introduction

Electrochromism is a phenomenon whereby the color of some transition-metal oxide materials can be changed reversibly by applying an electric field. Tungsten trioxide (WO_3) electrochromic materials have excellent optical modulation and cycle stability with good application prospects in energy conservation and artificial intelligence, such as smart windows, displays, anti-dazzle mirrors, and effective disguises [1–4]. Based on the electrochemical double injection/extraction of M^+ ions (small size cations, such as H^+, Li^+, Na^+, and K^+) and electrons, amorphous and crystalline WO_3 can be switched reversibly between the colored and bleached states by alternately applying a weak negative and positive voltage [5]. In comparison, nanostructured WO_3 films exhibit a larger surface area for ion diffusion and electron injection/extraction, along with a larger optical contrast ratio, faster switching speed, and higher coloration efficiency [6,7]. Many researchers have investigated the electrochromic properties of nanostructured WO_3 thin films.

Glancing angle deposition (GLAD), which involves manipulating the deposition angle and substrate rotation during the physical vapor deposition process, is a versatile nanofabrication technique based on the self-shadowing effect [8]. Nanostructures prepared by GLAD have the distinctive features of morphology sculpture, hetero-nanostructure design, and composition tenability by manipulating the nanoscale morphology and porosity, which also affect the film birefringence and dichroism [9,10]. Recently, considerable research has focused on nanostructured WO_3 electrochromic films fabricated by GLAD, and improvements in electrochromic performances have been discussed [11–15]. Beydaghyan et al. [14] found that the colored state of GLAD films exhibited an absorption- based coloration in the lower wavelengths as well as an increased reflection in the infrared region. Xiao et al. [12] successfully fabricated highly porous, oriented WO_3 nanocolumns on a flexible substrate by a facile electron-beam evaporation combined with the GLAD technique. Additionally, the electrochromic properties of WO_3 thin films have been studied under different annealing conditions [16–20]. Ng et al. [16] reported that WO_3 nanoplates annealed at 200 °C exhibited a high coloration efficiency, large optical modulation, and good electrochromic cycling stability, as well as short ions insertion and extraction cycles. Sallard et al. [17] demonstrated that sufficient crystallinity of WO_3 films was needed to ensure the cycling stability under realistic environmental conditions. Nevertheless, for nanostructured WO_3 films prepared by GLAD, the influence of annealing on the electrochromic properties are not well-explored. Our previous studies show that annealing treatment causes surface morphology degradation on GLAD films [21–23]. Therefore, the evolutions of the morphological, structural, and optical performances of WO_3 GLAD films under different annealing treatment should be investigated as well. Particularly, the electrochromic property

* Corresponding authors.
E-mail addresses: wangbinmars@siom.ac.cn (B. Wang), jdshao@mail.shcnc.ac.cn (J. Shao).

https://doi.org/10.1016/j.apsusc.2018.03.248
0169-4332/

of WO_3 GLAD thin films combining with the birefringence is worth pursuing further.

In this study, we present detailed research on WO_3-based thin films fabricated by GLAD. Firstly, the relatively optimal film thickness has been selected by comparing the film optical modulation. Then, morphologies, structures and optical properties are characterized. And the impacts of annealing temperatures on electrochromic properties of WO_3 nanostructured thin films are systematically investigated. Our results extend the knowledge into the tunable angular selective transmittance of tilted nanorods WO_3 films.

2. Experiments

2.1. Synthesis of nanostructured WO_3 films

Fluorine-doped tin oxide (FTO) glass substrates were ultrasonically cleaned in acetone and ethanol for 30 min. WO_3 films were deposited in an electron-beam evaporation chamber with GLAD manipulator [24]. The base pressure was $<1.5 \times 10^{-5}$ Torr, and the distance from the center of the substrates to the WO_3 (purity 99.9%) source material was maintained at 27 cm. With a flow rate of 200 sccm, WO_3 thin films were deposited in a 2-mTorr oxygen atmosphere. The deposition angle between the incident flux and the normal of substrate was set as 70° without rotation and heating. During the coating process, the deposition rate was maintained at approximately 0.25 nm/s via quartz crystal oscillator monitoring. Then, 900-, 500-, and 270-nm films were fabricated. The films were annealed at different temperatures (100, 200, 300, 350, and 400 °C) in air for 2 h at a heating rate of 100 °C·h^{-1} to consider the effect of the annealing temperature.

2.2. Characterizations

The morphologies of the WO_3 thin films were characterized by scanning electron microscopy (SEM, Hitachi S-4700). The crystallographic structures of the WO_3 films were characterized by X-ray diffraction (XRD, Empyrean, PANalytical), adopting a Rigaku D/MAX-2550 with Cu Kα (λ = 1.5408 Å). Raman spectra were measured in Renishaw Invia Raman Spectrometer under a 532.14-nm laser. X-ray photoelectron spectroscopy (XPS) was performed using an ESCALAB 250 (Thermo Scientific) with an Al Kα emission line at 1486.6 eV and an analyzer pass energy of 10 eV, and the spectra were analyzed using the commercial software Casa XPS. All binding energies were referenced to the C1s peak at 284.6 eV of the surface adventitious carbon to correct the shift caused by the charge effect.

2.3. Electrochemical and electrochromic evaluation

The electrochromic performances were obtained using a standard three-electrode, one-compartment electrochemical cell. The WO_3 film (Φ30 mm), a platinum sheet (35 mm × 35 mm), and Ag/AgCl (3.5 mol·L^{-1} KCl) were utilized as the working, counter, and reference electrodes, respectively. The electrolyte solution was hydrochloric acid (1 mol·L^{-1}). By applying voltages between −0.5 V and +0.5 V, chronoamperometry (CA) and cyclic voltammetry (CV) were performed using an electrochemical workstation (UN-O-16027, Zahhner Zennium). The transmittance spectra were measured in the spectral region between 300 and 1000 nm using an ultraviolet (UV)–visible (vis) spectrophotometer (Lambda 900). The p-polarized light transmittance of ±45° symmetry incidence was measured in the spectral region between 300 and 2000 nm.

3. Results and discussion

3.1. Thickness selection

As shown in Fig. 1, the thicker film of 900 nm exhibits a transmittance that is lower than expected because of the higher absorption. We chose films with thicknesses of 500 and 270 nm as subjects to study the transmittance modulation.

As a type of electrochromic material, the WO_3 film is transformed from the bleached state into the colored state by applying a negative voltage, which is represented as $WO_3 + xM^+ + xe^- \leftrightarrow M_x$-$WO_3$ [5], causing crystal structure variation. Then, electrons and cations are expelled out of intracell by applying a positive voltage, and the film changes to a transparent state [25]. Therefore, WO_3 thin films were subjected to a −0.5-V (or +0.5-V) voltage for 10 s to obtain the colored (or bleached) state, and transmittance spectra were measured in the spectral region between 300 and 1000 nm using the spectrophotometer.

As shown in Fig. 2, the transmittance shifts of the 500- and 270-nm films are 42.3% and 29.2% at 633 nm, respectively. However, the 270-nm film is too thin to store more cations and electrons; thus, the colored state of the 270-nm film exhibits a higher transmittance than that of the 500-nm film. Consequently, we shifted our focus to 500 nm as a relatively desirable thickness. According to Fig. 2, for the 500-nm WO_3 film, the transmittance of the colored state decreases with an increasingly negative applied voltage, indicating that a stronger negative voltage yields a larger charge capacity.

3.2. Structural analysis

WO_3 electrochromism is based on the electrochemical double insertion and extraction of electrons and cations, along with the phase transformation. WO_3 film crystallization affects the electrochromic performance as well. Although the structure and morphology of the WO_3 thin film has been considered to be the key roles in determining electrochromic properties [7,26], the influence of the annealing temperature for WO_3 thin films prepared by GLAD is still few reported.

XRD patterns for annealed WO_3 films are shown in Fig. 3. Obviously, no characteristic diffraction peaks of the as-grown sample are observed, which indicates that the as-grown film is in a fully amorphous state. Furthermore, the diffraction peaks of both the 350 °C-annealed sample and the 400 °C-annealed sample are sharp and intense, indicating their highly crystalline nature. No impurity peaks are observed, confirming the high purity of the two samples.

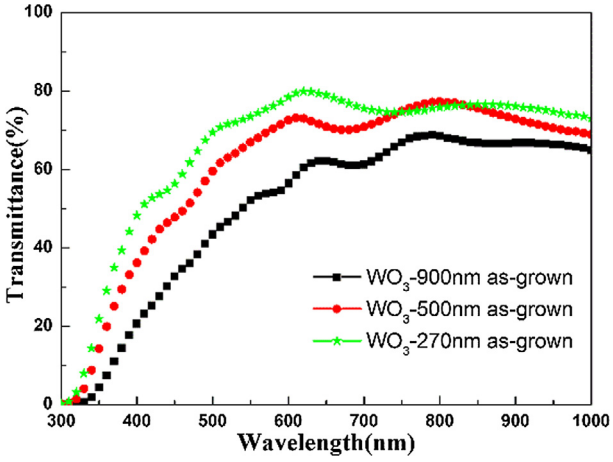

Fig. 1. Transmittance of WO_3 films with thicknesses of 900, 500, and 270 nm.

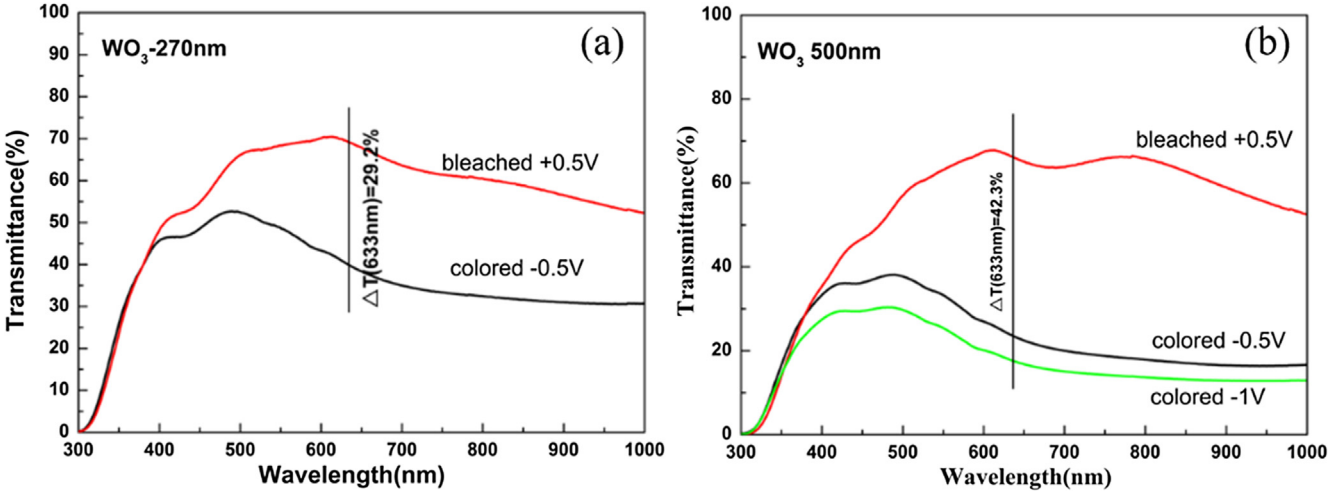

Fig. 2. Transmittance modulation of (a) 270- and (b) 500-nm WO_3 films.

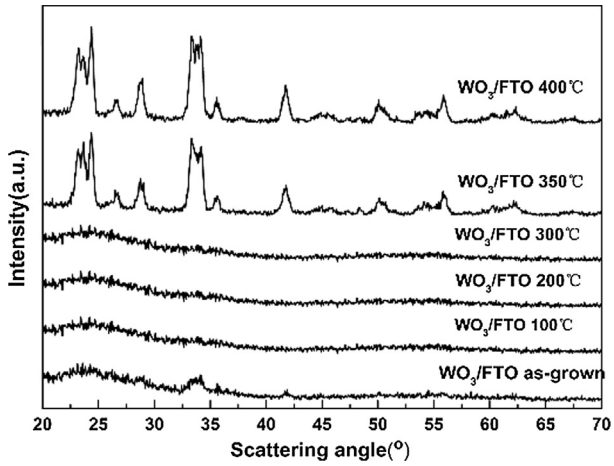

Fig. 3. XRD diffraction patterns of WO_3 films under different annealing conditions.

Therefore, the amorphous WO_3 film crystallizes around 350 °C, and the crystalline phases of both the 350 and 400 °C-annealed samples correspond to triclinic WO_3 (ICSD 80055, $P\bar{1}$ space group) [27].

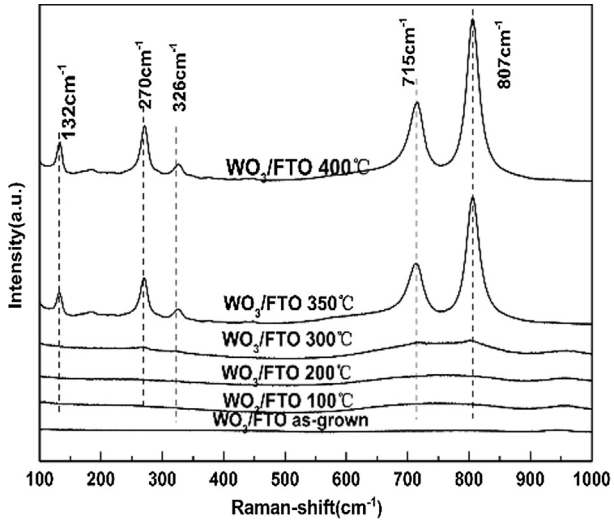

Fig. 4. Raman spectra of WO_3 films with different annealing treatments.

Fig. 4 shows the Raman spectra of WO_3 films annealed at different temperatures, which generally agree with the XRD patterns. Evidently, the WO_3 films transform from the amorphous state into the polycrystalline state when the annealing temperature increases to 350 °C. However, the Raman spectrum of the 300 °C-annealed sample exhibits weak peaks at 270, 328, 715, and 807 cm^{-1}. The characteristic positions of these peaks are in accordance with the fundamental mode of vibrations corresponding to the triclinic phase of WO_3 [28]. Apparently, the amorphous WO_3 film starts crystallizing at 300 °C.

3.3. Evolution of morphology

The top-view and cross-sectional SEM images of the WO_3 thin films in Figs. 5 and 6 show the surface morphologies and microstructures, respectively. The high-magnification SEM images shown in Fig. 6 indicate that the GLAD films consist of tilted and ordered WO_3 columns prepared at a deposition angle 70°. The unique microstructure of the WO_3 film can effectively increase the electrode/electrolyte contact areas and facilitate the electrons transfer and ions migration in the electrochemical reaction [29]. Along with the temperature increasing, the surface morphologies of the films change significantly. For example, consider the micropore size of the films in Fig. 5: the columns begin to agglomerate after the annealing treatment. Carefully examining the morphologies of films annealed at 100, 200, and 300 °C reveals that the columns are more tightly packed than those of the as-deposited sample, and the porosity of the samples decreases as the annealing temperature increases to 300 °C. However, the columnar structures of the films are separated by larger void regions with annealing temperature above 350 °C, as shown in Fig. 5(e) and (f). The porosity increase of the 350 °C-annealed sample is due to the higher-temperature treatment causing the columns to agglomerate more tightly and form larger void regions. Besides, the columns and the small grains on the columns clearly agglomerate, as shown in Fig. 5(f) and 6(f), indicating that the density of the sample increases after annealing at 400 °C. Messier et al. [30] demonstrated that these columns of GLAD films are composed of smaller microcolumn structures. Therefore, the morphology of GLAD films can be seriously influenced by the annealing treatment. The density of the WO_3 film varies as the annealing temperature increases because of the agglomeration of the columns and the crystallization of the material, which agrees with the results of our previous

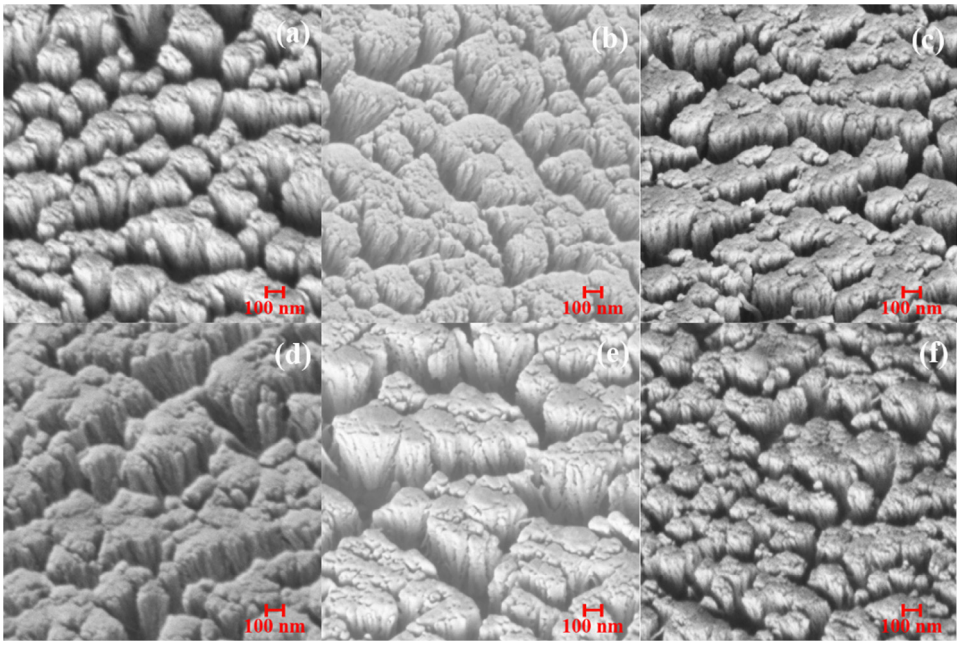

Fig. 5. Top-view images of WO_3 films with different annealing treatments: (a) as-grown, (b) 100 °C, (c) 200 °C, (d) 300 °C, (e) 350 °C, and (f) 400 °C.

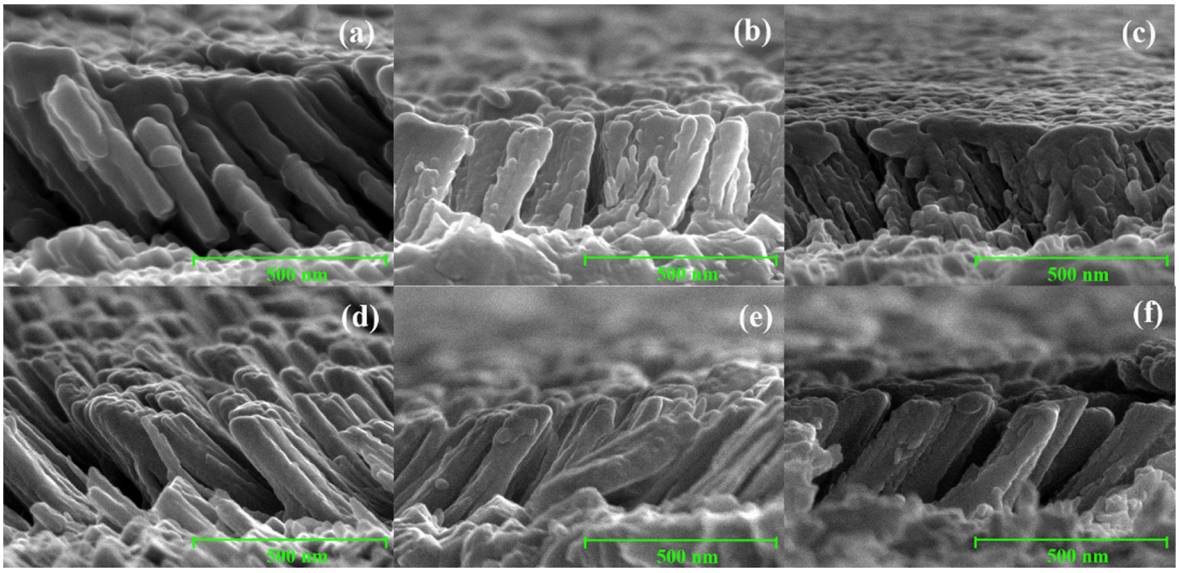

Fig. 6. Cross-sectional images of WO_3 films with different annealing treatments: (a) as-grown, (b) 100 °C, (c) 200 °C, (d) 300 °C, (e) 350 °C, and (f) 400 °C.

study concerning the morphology evolution of films prepared by GLAD under annealing treatment [22,23].

3.4. Chemical state analysis

XPS was used to characterize the surface composition and chemical states of WO_3. The W 4f core-level spectrum of the 400 °C-annealed WO_3 film exhibits two contributions: $4f_{5/2}$ and $4f_{7/2}$, located at 37.5 and 35.4 eV, respectively, as shown in Fig. 7 (a). This clearly indicates the presence of the six-valent tungsten (W^{6+}) oxidation state [31,32]. The W4f core-level peaks of WO_3 shift slightly (by approximately 0.4 eV) to lower binding energy side after the 400 °C annealing. Additionally, the W4f core-level peaks become sharper and more distinguishable above the annealing temperature of 350 °C. The O1s spectrum shown in Fig. 7(b) exhibits red shift as well. The shift is evidence of the chemical valence state transformation. The shift amounts of W4f and O1s depend on the oxygen-sufficient value, highlighting the oxygen-deficient state in the film annealed above 350 °C. Thus, the high-temperature annealing can partially reduce WO_3 but is too weak to significantly change the chemical valence state.

3.5. Electrochromic performances

The transmission spectra of WO_3 films annealed at different temperatures were measured using the UV–vis spectrophotometer in the spectral region between 300 and 1000 nm, as shown in Fig. 8. The results indicate that the as-grown WO_3 film has a relatively large optical modulation (42.2%, 633 nm). As the annealing temperature increases, the bleached-state transmittance of the annealed samples decreases gradually. The optical modulation decreases rapidly from 42.2% to 7.2% after the 400 °C annealing.

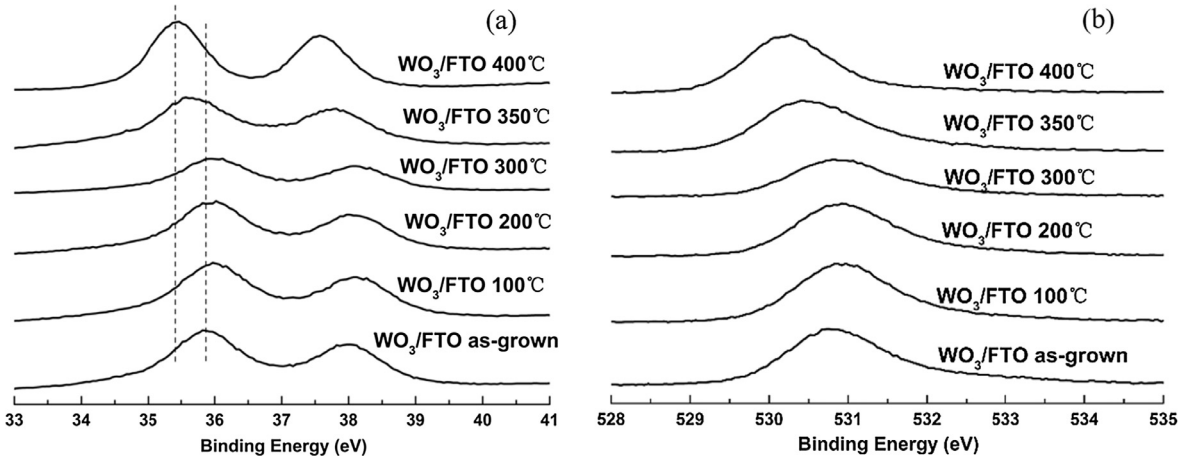

Fig. 7. XPS (a) W4f and (b) O1s spectra of WO_3 films with different annealing treatments.

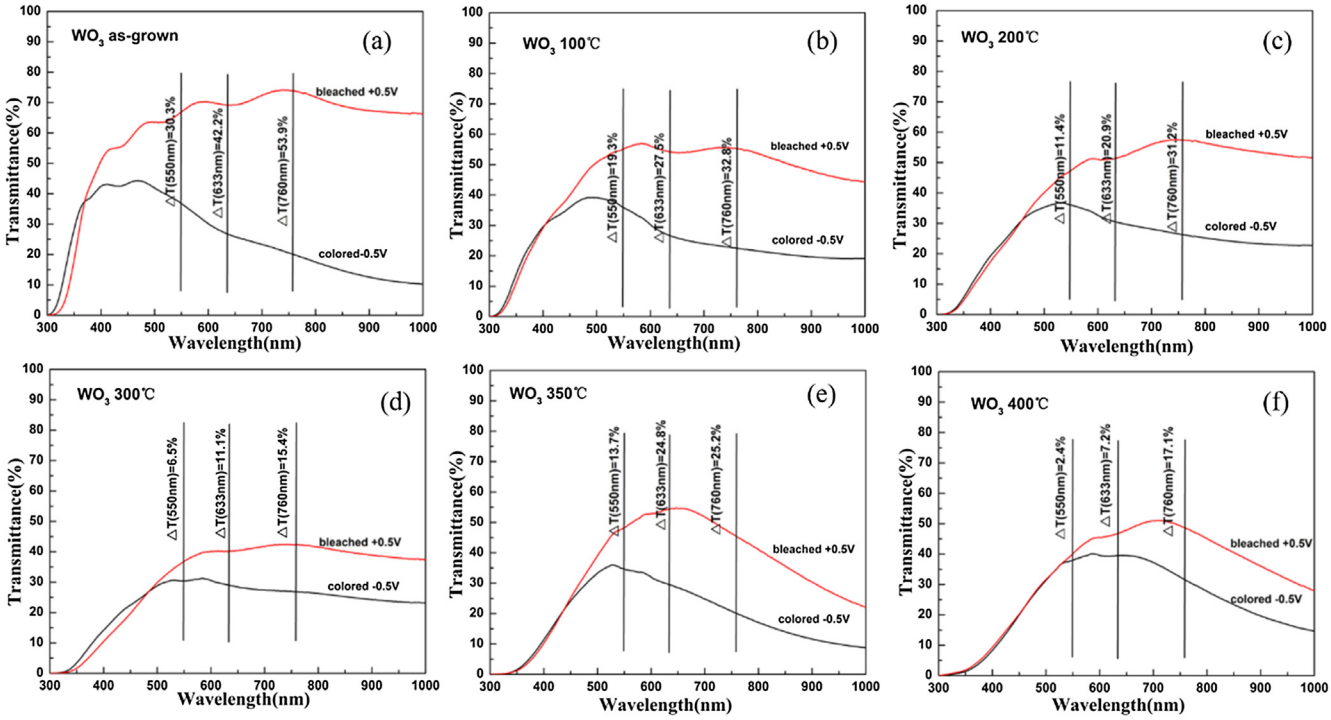

Fig. 8. Optical transmittance spectrum of WO_3 films with different annealing treatments: (a) as-grown, (b) 100 °C, (c) 200 °C, (d) 300 °C, (e) 350 °C, and (f) 400 °C.

The coloration/bleaching switching characteristics were recorded at 633 nm, as shown in Fig. 9. A small sudden bounce of the optical contrasts (%ΔT) appears at 350 °C, which is due to the slightly high bleached-state transmittance of the 350 °C-annealed sample. To explain this bounce, we consider the evolution of the porosity, which decreased initially and then increased as the annealing temperature increased, as shown in Fig. 5. The porosity of the samples after 100, 200, and 300 °C annealing gradually decreased because of the agglomeration of the columns. Consequently, the transmittance of the samples after 100, 200, and 300 °C annealing also decreased gradually, along with the film densities increasing. However, the void regions of film after 350 °C annealing is larger than that of the 200 and 300 °C-annealed samples; thus, the 350 °C-annealed sample shows a higher transmittance in the bleached state. Therefore, the small sudden bounce of the optical contrasts indicates good agreement between the porosity and transmissivity of the annealed samples. Besides, the optical modulation degraded significantly after 400 °C annealing. The colored-state transmittance and bleached-state transmittance of the 400 °C-annealed sample apparently increased and decreased, respectively, owing to the high-temperature annealing and WO_3 crystallization. High-temperature annealing changes the crystalline host lattice and increases the potential energy barriers, causing difficulty insert or extract ions sequentially. Consequently, the optical modulation of films under treatment at different temperatures is an outcome of the combined effects of the film porosity and crystallinity. The results demonstrate that the amorphous WO_3 film prepared by GLAD exhibited superior electrochromic performance to the crystalline WO_3 film [33,34].

Among the characteristic parameters determining the electrochromic properties, the cycling stability is regarded as one of the most important factors [35,36]. The CV curves in Fig. 10 show the cycling stability and degree of difficulty for ions transfer into films after 100 cycles. Obviously, the as-grown film has an optimal

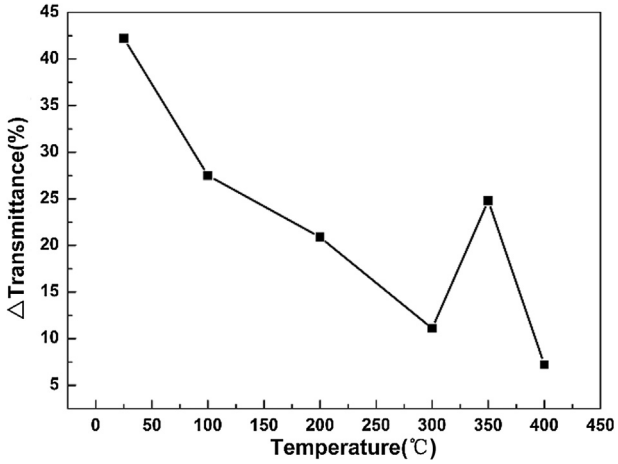

Fig. 9. Optical modulation of WO_3 films with different annealing treatments at 633 nm.

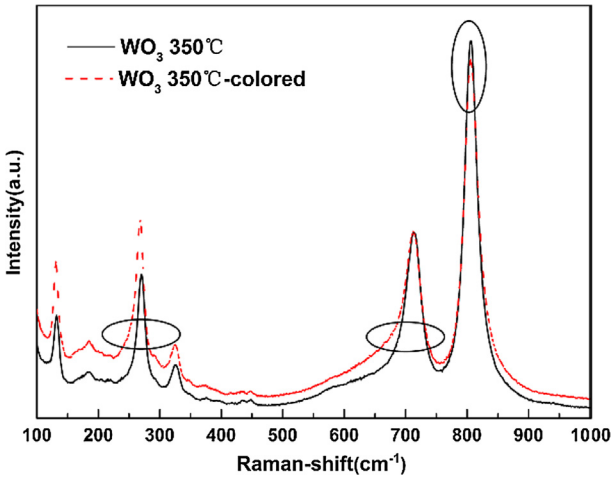

Fig. 11. Raman spectra of the colored and bleached states of the 350 °C-annealed sample. (For interpretation of the references to colour in this figure legend, the reader is referred to the web version of this article.)

charge capacity and better cycling stability than the annealed film. A significantly deterioration of the CV curve is observed as the annealing temperature increases, indicating that the annealing treatment reduces the charge capacity and redox reversibility. As the annealing temperature increases, the ordered lattice, the stable structure, and the increasing potential barriers of the ions intercalation can inhibit ion insertion and reduce the cycling stability [33]. As a result, the as-grown GLAD film has an optimal electrochromic property with a satisfactory cycling stability and large optical modulation, as the amorphous structure with defects is beneficial for ion insertion and extraction.

A Raman spectroscopic investigation of the colored and bleach states of the 350 °C-annealed sample was conducted to gain further insight into the structural changes. Raman spectroscopy has been proven as a powerful local structural probe for WO_3, as shown in Fig. 11. Specifically, all the peaks of the 350 °C-annealed film broaden significantly and exhibit a weak shift to a lower frequency (redshift) after the electrochromic reaction, and the peaks at the low frequency increase in intensity. All the data shown in Fig. 11 suggest that the stress fluctuation and phase transformation occur during the electrochromic reaction in the crystalline WO_3. The mechanism of electrochromism has long been controversial. The variation results of the Raman peaks indicate that internal stress fluctuation rather than phase transformation may dominate during the 350 °C-annealed film electrochromic reaction. Therefore, the specific mechanism remains to be further explored.

3.6. Angular selectivity

Major studies have focused on nanoscale materials for improving the electrochromic performance. However, the tilted nanocolumns thin film prepared by GLAD is characterized by birefringent characters [37–39]. Few studies have reported the unique optical nature of the birefringence for WO_3 GLAD thin films, which can result in angular selective transmittance [40,41]. Therefore, we investigated the angular selective transmittance of the as-grown

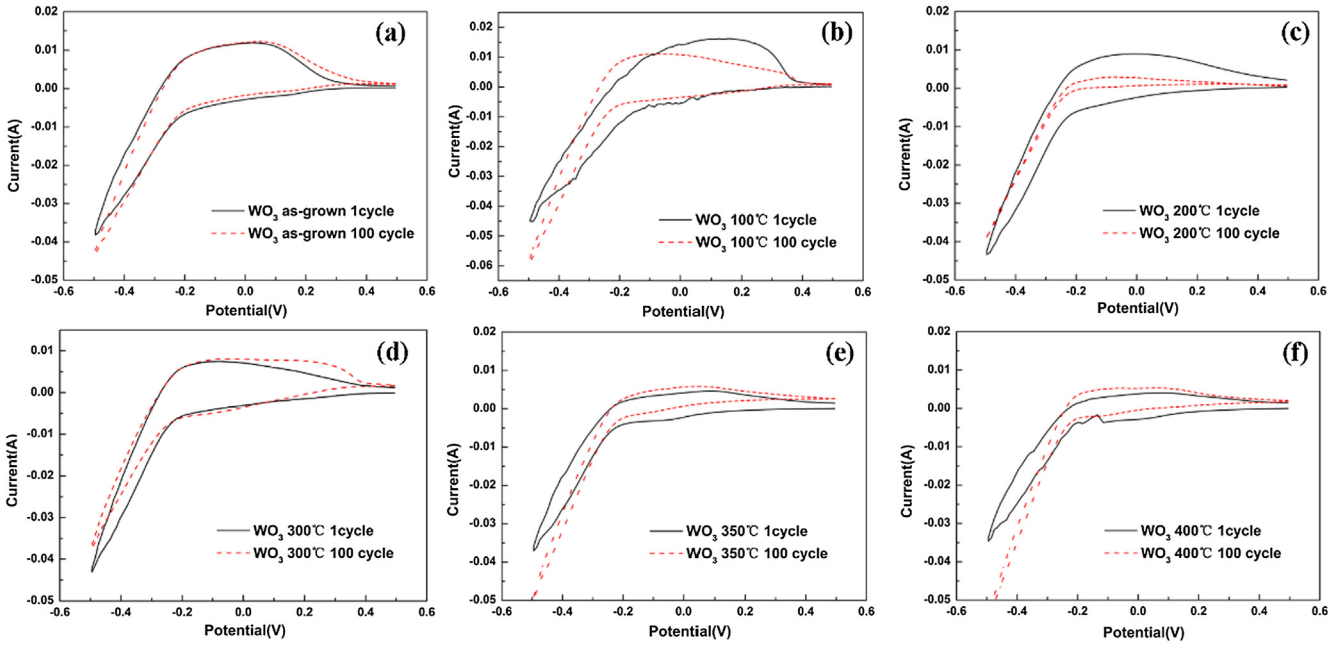

Fig. 10. CV curves of WO_3 films with different annealing treatments: (a) as-grown, (b) 100 °C, (c) 200 °C, (d) 300 °C, (e) 350 °C, and (f) 400 °C.

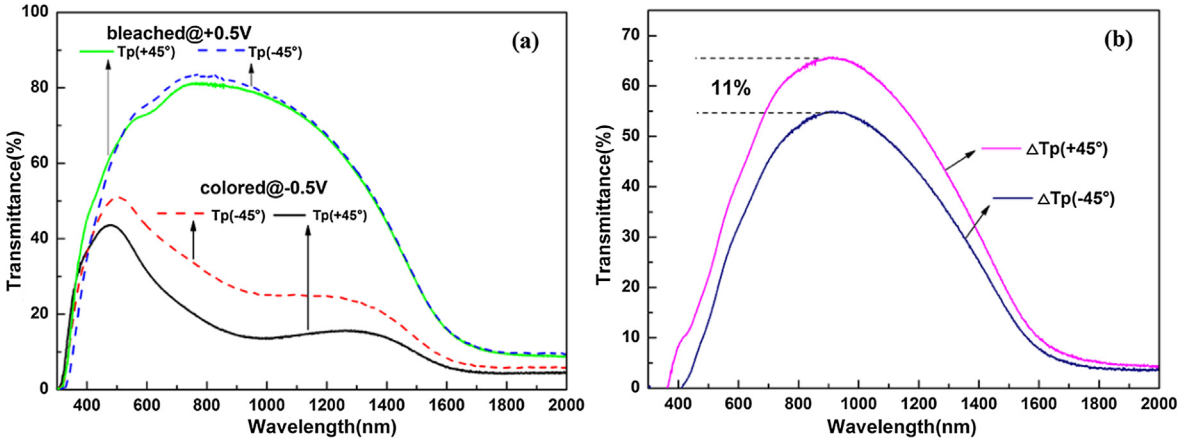

Fig. 12. Transmittance of WO_3 films under ±45° p-polarized light: (a) colored and bleached state; (b) optical contrasts (%ΔT). (For interpretation of the references to colour in this figure legend, the reader is referred to the web version of this article.)

GLAD WO_3 films in the electrochromic field. The detailed propagating theory, parameters, and regulation regarding the symmetry incidence can be found in the literature [21,39].

As shown in Fig. 12, under illumination with p-polarized light at ±45° symmetry incidence (in the case of the incident plane coinciding with the vapor incidence plane), the spectrum curves of the colored state are not exactly consistent with that of the bleached state. From Fig. 12(a), the angular selectivity of the colored states exhibits a larger modulation than that of the bleached states, which is attributed to the absorption increase of the colored states. The optical contrasts (%ΔT) of as-grown GLAD WO_3 films at +45° and −45° incidence in the vis–IR region are shown in Fig. 12(b). The difference of the transmittance modulation contrast for the p-polarized light between the +45° and −45° incidence can be up to 11%. Apparently, the WO_3 thin film shows a relatively large optical modulation in the vis and near-IR region (1000–1400 nm), but the optical modulation in the IR region (>1600 nm) is small. Nonetheless, the doping modification is a feasible proposal for improving the transmittance modulation performance in the IR region. The optical transmittance contrasts of the colored states under the p-polarized light with ±45° incidence obtained by applying different voltages are shown in Fig. 13. In the 400–1000-nm region, the transmittance decreases significantly at the voltage of −1 V owing to the more H^+-ion insertion. As indicated by the optical modulation in Fig. 13, the angular selectivity of the GLAD WO_3 films with the unique microstructure could be adjusted by applying different voltages. Therefore, the special performance of the tilted columnar electrochromic films provides new application features and development potential.

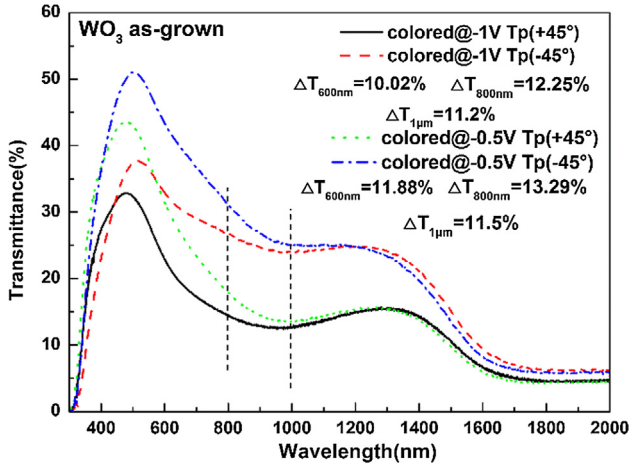

Fig. 13. Optical transmittance contrasts (%ΔT) of the colored state under ±45° p-polarized light with different applied voltages. (For interpretation of the references to colour in this figure legend, the reader is referred to the web version of this article.)

4. Conclusion

WO_3 thin films were fabricated by glancing angle deposition technique (GLAD) and annealed at different temperatures. The WO_3 films begin to crystallize at around 300 °C. Comparing with the annealed films, the as-grown GLAD WO_3 film exhibits relatively optimum electrochromic properties, along with a satisfactory cycling stability and large optical modulation (42.2%, 633 nm), because the loose structure facilitated fast ion diffusion and rapid color alteration. Furthermore, a noteworthy feature of tilted columnar structured films is that under illumination with p-polarized light, the transmittance modulation contrast between the +45° and −45° incidence can be up to 11%. The angular selectivity of the colored and bleached states of GLAD WO_3 films illuminated with p-polarized light can be tuned by applying different voltages, which provides new application features and development potential.

Acknowledgements

This work was supported by the CAS Interdisciplinary Innovation Team and National Natural Science Foundation of China (Grant No.11535010).

References

[1] C.G. Granqvist, Handbook of Inorganic Electrochromic Materials, Elsevier, 1995.
[2] A. Llordés, G. Garcia, J. Gazquez, D.J. Milliron, Tunable near-infrared and visible-light transmittance in nanocrystal-in-glass composites, Nature 500 (2013) 323–326.
[3] J. Chou, Y. Liao, C. Huang, C. Liu, S. Yang, M. Su, C. Yang, C. Huang, P. Ho, A study on electrochemical and optical characteristics of WO_{1-x} electrochromic thin film prepared by different constant potentials and deposition time, Physica E 44 (2012) 1467.
[4] A.V. Kadam, Propylene glycol-assisted seed layer-free hydrothermal synthesis of nanostructured WO_3 thin films for electrochromic applications, J. Appl. Electrochem. 47 (2017) 335.
[5] B.W. Faughnan, R.S. Crandall, P.M. Heyman, Electrochromism in tungsten (VI) oxide amorphous films, RCA Rev. 36 (1975) 177–197.
[6] H. Lia, J. Wang, Q. Shia, M. Zhang, Ch. Hou, G. Shi, H. Wang, Q. Zhang, Y. Li, Q. Chi, Constructing three-dimensional quasi-vertical nanosheet architectures from self-assemble two-dimensional $WO_3{\cdot}2H_2O$ for efficient electrochromic devices, Appl. Surf. Sci. 380 (2016) 281–287.

[7] M. Layani, P. Darmawan, W. Foo, L. Liu, A. Kamyshny, D. Mandler, S. Magdassi, P.S. Lee, Nanostructured electrochromic films by inkjet printing on large area and flexible transparent silver electrodes, Nanoscale 6 (2014) 4572–4576.
[8] D. Deniz, D.J. Frankel, R.J. Lad, Nanostructured tungsten and tungsten trioxide films prepared by glancing angle deposition, Thin Solid Films 518 (2010) 4095–4099.
[9] J. Lee, K. Park, T. Kim, H. Choi, Y. Sung, Controlled growth of high-quality TiO_2 nanowires on sapphire and silica, Nanotechnology 17 (2016) 4317–4321.
[10] J.J. Steele, M.J. Brett, Nanostructure engineering in porous columnar thin films: recent advances, J. Mater. Sci: Mater. Electron. 18 (2007) 367–379.
[11] J. Gil-Rostra, M. Cano, J. Pedrosa, F.J. Ferrer, F. García-García, F. Yubero, A.R. González-Elipe, Electrochromic behavior of $W_xSi_yO_z$ thin films prepared by reactive magnetron sputtering at normal and glancing angles, ACS Appl. Mater. Interfaces 4 (2012) 628–638.
[12] L. Xiao, Y. Lv, W. Dong, N. Zhang, X. Liu, Dual-functional WO_3 nanocolumns with broadband antireflective and high-performance flexible electrochromic properties, ACS Appl. Mater. Interfaces 8 (2016) 27107–27114.
[13] G. Beydaghyan, G. Bader, P.V. Ashrit, Electrochromic and morphological investigation of dry-lithiated nanostructured tungsten trioxide thin films, Thin Solid Films 516 (2008) 1646–1650.
[14] G. Beydaghyan, J.M. Renaud, G. Bader, P.V. Ashrit, Enhanced electrochromic properties of heat treated nanostructured tungsten trioxide thin films, J. Master. Res. 23 (2008) 274–280.
[15] G. Beydaghyan, M. Boudreau, P.V. Ashrit, Optical properties and electrochromic response of nanostructured molybdenum trioxide films, J. Mater. Res. 26 (2011) 55–61.
[16] C.Y. Nga, K.A. Razaka, Z. Lockman, Effect of annealing on acid-treated $WO_3{\cdot}H_2O$ nanoplates and their electrochromic properties, Electrochimica Acta 178 (2015) 673–681.
[17] S. Sallard, T. Brezesinski, B.M. Smarsly, Electrochromic stability of WO_3 thin films with nanometer-scale periodicity and varying degrees of crystallinity, J. Phys. Chem. C 111 (2007) 7200–7206.
[18] J. Xue, Y. Zhu, M. Jiang, J.n. Su, Y. Liu, Electrochromic WO_3 thin films prepared by combining ion-beam sputtering deposition with post-annealing, Mater. Lett. 149 (2015) 127–129.
[19] R. Sivakumara, R. Gopalakrishnanb, M. Jayachandranc, C. Sanjeeviraja, Preparation and characterization of electron beam evaporated WO_3 thin films, Opt. Mater. 29 (2007) 679–687.
[20] D. Chatzikyriakoua, A. Mahoa, R. Cloots, C. Henrist, Ultrasonic spray pyrolysis as a processing route for templated electrochromic tungsten oxide films, Microporous Mesoporous Mater. 240 (2017) 31–38.
[21] B. Wang, H. Qi, H. Wang, Y. Cui, J. Guo, Y. Cui, Y. Liu, K. Yi, J. Shao, Morphology, structure and optical properties in TiO_2 nanostructured films annealed at various temperatures, Opt. Mater. Express 5 (2015) 1410–1418.
[22] B. Wang, H. Qi, Y. Chai, M. Li, M. Guo, M. Pan, H. Wang, Y. Cui, J. Shao, Alteration of titanium dioxide material properties by glancing angle deposition plus annealing treatment, Superlattices Microstruct. 90 (2016) 87–95.
[23] B. Wang, H. Qi, Z. Liu, Y. Jin, H. Wang, Y. Chai, J. Yuan, J. Zhao, J. Shao, Structure, chemical state and photocatalytic activity of TiO_{2-x} nanostructured thin films by glancing angle deposition technique, J. Alloys Compd. 716 (2017) 299–305.
[24] Y. Zhao, Dynamic shadowing growth and its energy applications, Front. Energy Res. 2 (2014) 1–8.
[25] W. Man, H. Lu, L. Ju, F. Zheng, M. Zhanga, M. Guo, Effect of substrate pre-treatment on microstructure and enhanced electrochromic properties of WO_3 nanorod arrays, RSC Adv. 5 (2015) 106182–106190.
[26] Y. Liu, Y. Lv, Z. Tang, L. He, X. Liu, Highly stable and flexible ITO-free electrochromic films with Bi-functional stacked MoO_3/Ag/MoO_3, structures, Electrochim. Acta 189 (2016) 184–189.
[27] P.M. Woodward, A.W. Sleight, T. Vogt, Structure refinement of triclinic tungsten trioxide, J. Phys. Chem. Solid 56 (1995) 1305–1315.
[28] C. Santato, M. Odziemkowski, M. Ulmannn, J. Augustynski, Crystallographically oriented mesoporous WO_3 films: synthesis, characterization, and applications, J. Am. Chem. Soc. 123 (2001) 10639–10649.
[29] J.M. Wang, E. Khoo, P.S. Lee, J. Ma, Controlled synthesis of WO_3 nanorods and their electrochromic properties in H_2SO_4 electrolyte, J. Phys. Chem. C 113 (2009) 9655–9658.
[30] R. Messier, A.P. Giri, R.A. Roy, Revised structure zone model for thin film physical structure, J. Vac. Sci. Technol. A 2 (1984) 500–503.
[31] C. Sunseri, F. Di Quarto, A. Di Paola, Kinetics of coloration of anodic electrochromic films of $WO_3{\cdot}H_2O$, J. Appl. Electrochem. 10 (1980) 669.
[32] C.S. Blackman, I.P. Parkin, Atmospheric pressure chemical vapor deposition of crystalline monoclinic WO_3 and WO_{3-x} thin films from reaction of WCl_6 with O-containing solvents and their photochromic and electrochromic properties, Chem. Mater. 17 (2005) 1583.
[33] Y. Yang, Y. Cao, B. Loo, J. Yao, Microstructures of electrochromic MoO_3 thin films colored by injection of different cations, J. Phys. Chem. B 102 (1998) 9392–9396.
[34] M. Laurenti, S. Bianco, M. Castellino, N. Garino, A. Virga, C.F. Pirri, P. Mandracci, Toward plastic smart windows: optimization of indium tin oxide electrodes for the synthesis of electrochromic devices on polycarbonate substrates, ACS Appl. Mater. Interfaces 8 (2016) 8032–8042.
[35] D. Ma, G. Shi, H. Wang, Q. Zhang, Y. Li, Morphology-tailored synthesis of vertically aligned 1DWO_3 nano-structure films for highly enhanced electrochromic performance, J. Mater. Chem. A 1 (2013) 684–691.
[36] J. Wang, E. Khoo, P.S. Lee, J. Ma, Synthesis, assembly, and electrochromic properties of uniform crystalline WO_3 nanorods, J. Phys. Chem. C 112 (2008) 14306–14312.
[37] T. Motohiro, Y. Taga, Thin film retardation plate by oblique deposition, Appl. Opt. 28 (1989) 2466–2482.
[38] Y. Hou, H. Qi, K. Yi, J. Shao, Analysis of angular-selective performances of obliquely deposited birefringent thin film, Chin. Opt. Lett. 11 (2013) 103101.
[39] B. Wang, H. Qi, H. Wang, Y. Chai, W. Sun, Y. Hou, K. Yi, J. Shao, Novel theory analysis and new perspective on angular selectivity, Opt. Commun. 325 (2014) 1–4.
[40] G. Mbise, G.A. Niklasson, C.G. Granqvist, S. Palmer, Angular-selective window coatings: theory and experiment, Opt. Mater. Energy Effic. Sol. Energy Convers. 2103 (1989) 179–199.
[41] G. Mbise, G.A. Niklasson, C.G. Granqvist, Obliquely evaporated Cr films with large angular selectivity, J. Appl. Phys. 77 (1995) 1816–2818.